Author(s): Hinkkanen, M. & Luomi, J.

Title: Stabilization of Regenerating-Mode Operation in Sensorless Induction Motor Drives by Full-Order Flux Observer Design

Year: 2004

Version: Post print

Please cite the original version:

Hinkkanen, M. & Luomi, J. 2004. Stabilization of Regenerating-Mode Operation in Sensorless Induction Motor Drives by Full-Order Flux Observer Design. IEEE Transactions on Industrial Electronics. Volume 51, Issue 6. 1318-1328. ISSN 0278-0046 (printed). DOI: 10.1109/tie.2004.837902.

Stabilization of Regenerating-Mode Operation in Sensorless Induction Motor Drives by Full-Order Flux Observer Design

Marko Hinkkanen and Jorma Luomi, *Member, IEEE*

***Abstract*—This paper deals with the full-order flux observer design for speed-sensorless induction motor drives. An unstable region encountered in the regenerating mode at low speeds is well known. To remedy the problem, a modified speed-adaptation law is proposed. Instead of using only the current estimation error perpendicular to the estimated flux, the parallel component is also exploited in the regenerating mode. Using current estimation error loci in steady state, a linearized model, simulations, and experiments, it is shown that the observer using the proposed speed-adaptation law does not have the unstable region. It is also shown that the effect of erroneous parameter estimates on the accuracy of the observer is comparatively small.**

***Index Terms*—Full-order flux observer, induction motor drives, speed sensorless, stability analysis.**

I. Introduction

Speed-sensorless induction motor drives have developed significantly during the last few years. Speed-adaptive full-order flux observers [1], [2] are promising flux estimators for induction motor drives. The speed-adaptive observer consists of a state-variable observer augmented with a speed-adaptation loop. The observer gain and the speed-adaptation law determine the properties of the observer. Dynamic performance comparable to drives equipped with a speed sensor can be achieved in a wide speed and load range. However, induction motor drives using the conventional speed-adaptive flux observer become unstable when regenerating at low speed [3], [4], [5]. Speed-sensorless reduced-order observers also have similar problems in the regenerating mode [6]. As shown in [7], the speed and fluxes of the machine are observable from stator quantities at all operating points except dc excitation. Thus the instability of the conventional observer is due to inadequate observer design.

The conventional speed-adaptation law is based on the component of the current estimation error which is perpendicular to the estimated rotor flux. The adaptation law was originally derived using the Lyapunov stability theory [1] or the Popov hyperstability theory [2]. However, the stability of the adaptation law is not guaranteed. The derivation in [1] neglects a term including the actual rotor flux (which is not measurable) as shown in [4]. The positive-realness condition is not satisfied in [2] as shown in [3]. A speed-adaptation law based on the current estimation error perpendicular to the estimated stator flux was proposed in [8]. The adaptation law was derived using the Lyapunov stability theory. However, the stability is not guaranteed as shown in Appendix A, and stability problems still exist in the regenerating mode.

The authors of [1] realized the problem in their original design and proposed a solution in [5], where the regenerating mode is stabilized by the observer gain design. An observer gain design reducing the unstable region was considered in [3]. An alternative approach to remedy the instability is to modify the speed-adaptation law. A new speed-adaptation law was proposed in [7], where the error angle between the modified current vector and its estimate is used. However, the effect of parameter errors was not studied in [3], [5], and the study in [7] indicated problems in no-load operation when the stator resistance estimate is erroneous.

This paper proposes a modified speed-adaptation law where the projection of the current estimation error is changed in the regenerating-mode low-speed operation. The induction motor model and the speed-adaptive flux observer are first defined. Then, loci of the current estimation error in steady state are used to clarify the problem and its solution. The stability is studied by using pole plots of the linearized system. The proposed observer is compared with three existing solutions by studying the effects of parameter errors on the accuracy. Finally, after describing a control system based on the rotor flux orientation, simulation and experimental results are presented.

II. Induction Motor Model

The parameters of the inverse-Γ-equivalent circuit [9] of an induction motor are the stator resistance R_s, the rotor resistance R_R, the stator transient inductance L'_s, and the magnetizing inductance L_M. The electrical angular speed of the rotor is denoted by ω_m, the angular speed of the reference frame by ω_k, the stator current space vector by $\underline{i}_s$, and the stator voltage by $\underline{u}_s$. When the stator flux $\underline{\psi}_s$ and the rotor flux $\underline{\psi}_R$ are chosen as state variables, the state-space representation of the induction motor becomes

$$\underline{\dot{\mathbf{x}}} = \underbrace{\begin{bmatrix} -\frac{1}{\tau'_s} - j\omega_k & \frac{1}{\tau'_s} \\ \frac{1-\sigma}{\tau'_r} & -\frac{1}{\tau'_r} - j\left(\omega_k - \omega_m\right) \end{bmatrix}}_{\mathbf{A}} \underline{\mathbf{x}} + \underbrace{\begin{bmatrix} 1 \\ 0 \end{bmatrix}}_{\mathbf{B}} \underline{u}_s \tag{1a}$$

$$\underline{i}_s = \underbrace{\begin{bmatrix} \frac{1}{L'_s} & -\frac{1}{L'_s} \end{bmatrix}}_{\mathbf{C}} \underline{\mathbf{x}} \tag{1b}$$

The authors are with the Power Electronics Laboratory, Helsinki University of Technology, FIN-02015 HUT, Espoo, Finland (email: marko.hinkkanen@hut.fi; jorma.luomi@hut.fi).

TABLE I
PARAMETERS OF 2.2-KW 4-POLE 400-V 50-HZ MOTOR AND LOAD

Stator resistance R_s	3.67 Ω
Rotor resistance R_R	2.10 Ω
Magnetizing inductance L_M	0.224 H
Stator transient inductance L'_s	0.0209 H
Rated speed	1 430 r/min
Rated current	5.0 A
Rated torque	14.6 Nm
Total moment of inertia	0.0155 kgm^2
Viscous friction coefficient	0.0025 Nm·s

where the state vector is $\underline{\mathbf{x}} = [\underline{\psi}_s \quad \underline{\psi}_R]^T$, and the parameters are $\sigma = L'_s/(L_M + L'_s)$, $\tau'_s = L'_s/R_s$, and $\tau'_r = \sigma L_M/R_R$. The electromagnetic torque is

$$T_e = \frac{3}{2}p\,\mathrm{Im}\left\{\underline{i}_s\underline{\psi}^*_R\right\} = \frac{3}{2}p\frac{1}{L'_s}\,\mathrm{Im}\left\{\underline{\psi}_s\underline{\psi}^*_R\right\} \tag{2}$$

where p is the number of pole pairs and the complex conjugates are marked by the symbol *. In this paper, the parameters of a 2.2-kW four-pole induction motor given in Table I are used.

III. SPEED-ADAPTIVE FULL-ORDER FLUX OBSERVER

Choosing the stator and rotor fluxes as state variables is preferred since no inductance derivatives are needed and the modelling of magnetic saturation becomes simpler. In addition, the observer could be used with stator flux orientation control or direct torque control [8] as well as with rotor flux orientation control. Consequently, the full-order flux observer is defined by

$$\dot{\underline{\hat{\mathbf{x}}}} = \underline{\hat{\mathbf{A}}}\,\underline{\hat{\mathbf{x}}} + \mathbf{B}\underline{u}_s + \underline{\mathbf{L}}\big(\underline{i}_s - \underline{\hat{i}}_s\big) \tag{3a}$$

$$\underline{\hat{i}}_s = \mathbf{C}\underline{\hat{\mathbf{x}}} \tag{3b}$$

where the observer state vector is $\underline{\hat{\mathbf{x}}} = [\underline{\hat{\psi}}_s \quad \underline{\hat{\psi}}_R]^T$ and the estimates are marked by the symbol $\hat{}$. The matrix $\underline{\hat{\mathbf{A}}}$ and the observer gain $\underline{\mathbf{L}}$ are given by

$$\underline{\hat{\mathbf{A}}} = \begin{bmatrix} -\frac{1}{\tau'_s} - j\omega_k & \frac{1}{\tau'_s} \\ \frac{1-\sigma}{\tau'_r} & -\frac{1}{\tau'_r} - j(\omega_k - \hat{\omega}_m) \end{bmatrix}, \quad \underline{\mathbf{L}} = \begin{bmatrix} \underline{l}_s \\ \underline{l}_r \end{bmatrix} \tag{3c}$$

It is desired to have a wide speed and torque range with good dynamic properties. The approach used in this paper is to design the observer gain especially for nominal and high-speed operation whereas the problems at low speeds are handled by modifying the speed-adaptation law.

A. Observer Gain

A simple observer gain giving fast and well-damped observer dynamics up to very high speeds is adopted [10]

$$\underline{\mathbf{L}} = \lambda \begin{bmatrix} 1 + j\,\mathrm{sign}(\hat{\omega}_m) \\ -1 + j\,\mathrm{sign}(\hat{\omega}_m) \end{bmatrix} \tag{4a}$$

where

$$\lambda = \begin{cases} \lambda' \frac{|\hat{\omega}_m|}{\omega_\lambda}, & \text{if } |\hat{\omega}_m| < \omega_\lambda \\ \lambda', & \text{if } |\hat{\omega}_m| \geq \omega_\lambda \end{cases} \tag{4b}$$

Parameters λ' and ω_λ are positive constants. The parameter λ' can be considered as an impedance, which may be helpful when choosing λ' for different motor sizes. In this paper, the observer gain is determined by $\lambda' = 10\ \Omega$ and $\omega_\lambda = 1$ p.u. The base value of the angular frequency is $2\pi{\cdot}50\ \mathrm{s}^{-1}$.

B. Speed-Adaptation Laws

The rotor speed estimate is obtained using the adaptation mechanism

$$\hat{\omega}_m = -\gamma_p\,\varepsilon - \gamma_i \int \varepsilon\,dt \tag{5}$$

where γ_p and γ_i are positive adaptation gains and ε is an error term. Due to integral action of (5), the error term is driven to zero in steady state. The gains $\gamma_p = 10\ (\mathrm{Nm{\cdot}s})^{-1}$ and $\gamma_i = 10\,000\ (\mathrm{Nm{\cdot}s^2})^{-1}$ are used in this paper.

1) Conventional: The error term of the conventional speed-adaptation law is

$$\varepsilon = \mathrm{Im}\left\{\big(\underline{i}_s - \underline{\hat{i}}_s\big)\underline{\hat{\psi}}^*_R\right\} \tag{6}$$

Only the current estimation error perpendicular to the estimated rotor flux is used to estimate the speed. The adaptation law works well except in the regenerating mode at low speeds.

2) Proposed: The proposed error term is

$$\varepsilon = \mathrm{Im}\left\{\big(\underline{i}_s - \underline{\hat{i}}_s\big)\underline{\hat{\psi}}^*_R e^{-j\phi}\right\} \tag{7}$$

where the angle ϕ changes the direction of the error projection. In other words, the component of the current estimation error parallel to the estimated rotor flux is also exploited when $\phi \neq 0$. The angle ϕ can be used to stabilize the regenerating-mode operation at low speeds.

IV. LOCI OF CURRENT ESTIMATION ERROR IN STEADY STATE

Based on (1) and (3), the estimation error $\underline{\mathbf{e}} = \underline{\mathbf{x}} - \underline{\hat{\mathbf{x}}}$ of the state vector and the estimation error of the stator current are

$$\dot{\underline{\mathbf{e}}} = (\underline{\mathbf{A}} - \underline{\mathbf{L}}\mathbf{C})\,\underline{\mathbf{e}} + \begin{bmatrix} 0 \\ j\underline{\hat{\psi}}_R \end{bmatrix}(\omega_m - \hat{\omega}_m) \tag{8a}$$

$$\underline{i}_s - \underline{\hat{i}}_s = \mathbf{C}\underline{\mathbf{e}} \tag{8b}$$

respectively. In the following, accurate motor parameter estimates are assumed. The estimation error $\underline{\mathbf{e}}$ is considered in steady state, i.e., $\dot{\underline{\mathbf{e}}} = 0$. This assumption is reasonable if the estimation error $\underline{\mathbf{e}}$ is changing much faster than ω_m and $\hat{\omega}_m$. The steady-state solution of the current estimation error becomes

$$\underline{i}_s - \underline{\hat{i}}_s = \frac{\underline{\hat{\psi}}_R\,(\omega_m - \hat{\omega}_m)}{\left(\frac{\sigma}{\tau'_r} + j\omega_r\right)\frac{R_s + l_s}{\omega_s} + jL'_s\left(\frac{1}{\tau'_r} - \frac{l_r}{L'_s} + j\omega_r\right)} \tag{9}$$

where ω_s is the angular frequency of the estimated rotor flux (which corresponds to the stator frequency in steady state) and $\omega_r = \omega_s - \omega_m$ is the angular slip frequency. The estimated rotor flux reference frame is used, i.e., $\omega_k = \omega_s$ and $\underline{\hat{\psi}}_R = \hat{\psi}_R + j0$. Based on (9), the current estimation error in steady state can be easily calculated for a given error $\omega_m - \hat{\omega}_m$ and an operating point determined by ω_s, ω_r, and $\hat{\psi}_R$. The results of this section are augmented by analyzing the linearized observer in Section V.

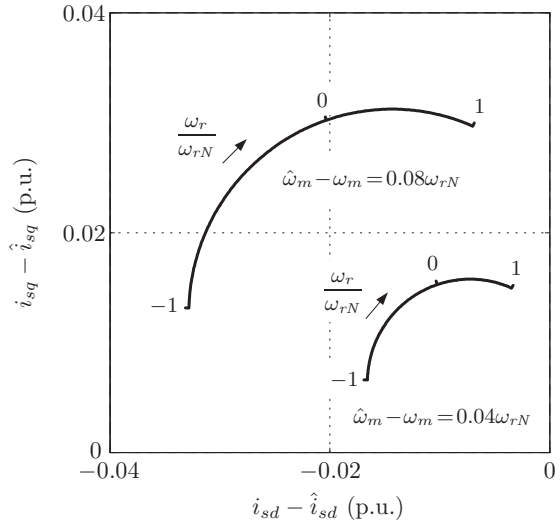

Fig. 1. Loci of current estimation error when angular slip frequency ω_r varies from negative rated slip to positive rated slip (rated angular slip frequency being $\omega_{rN} = 0.05$ p.u.). Angular stator frequency is $\omega_s = 0.1$ p.u., and results for two different speed estimation errors ($0.04\omega_{rN}$ and $0.08\omega_{rN}$) are shown. Estimated rotor flux reference frame is used.

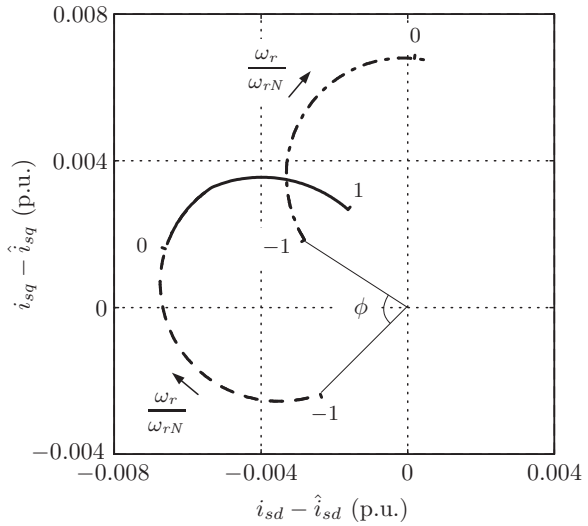

Fig. 2. Loci of current estimation error when angular slip frequency ω_r varies from negative rated slip to positive rated slip. Angular stator frequency is $\omega_s = 0.01$ p.u. and speed estimation error is $\hat{\omega}_m - \omega_m = 0.04\omega_{rN}$. Locus consisting of dashed curve and solid curve corresponds to conventional adaptation law. Locus consisting of dash-dotted curve and solid curve corresponds to proposed adaptation law. Estimated rotor flux reference frame is used.

A. Stable Region

The loci of current estimation error for two different speed estimation errors are depicted in Fig. 1 when the angular slip frequency ω_r varies from the negative rated slip to the positive rated slip (the rated angular slip frequency being $\omega_{rN} = 0.05$ p.u.). The angular stator frequency is $\omega_s = 0.1$ p.u. In the estimated rotor flux reference frame, the stator current is $\underline{i}_s = i_{sd} + ji_{sq}$. It can be seen that the larger the speed error, the larger is the current estimation error. In Fig. 1, $\omega_s > 0$ and $\hat{\omega}_m > \omega_m$. If $\omega_s < 0$, the loci lie in the right half-plane. If $\hat{\omega}_m < \omega_m$, the loci are located in the lower half-plane.

In the estimated rotor flux reference frame, the error term (6) corresponding to the conventional adaptation law reduces to

$$\varepsilon = (i_{sq} - \hat{i}_{sq})\hat{\psi}_R \tag{10}$$

The speed estimate (5) thus depends on the error $i_{sq} - \hat{i}_{sq}$. If $\hat{\omega}_m > \omega_m$, the condition $i_{sq} - \hat{i}_{sq} > 0$ should hold in order the speed estimate to converge. In Fig. 1, this condition holds for all slip frequencies including the regenerating-mode operation (where $\omega_s\omega_r < 0$).

B. Unstable Region

Loci of the current estimation error for a lower angular stator frequency $\omega_s = 0.01$ p.u. are shown in Fig. 2. The locus consisting of the dashed curve and the solid curve shows the current estimation error. The condition $i_{sq} - \hat{i}_{sq} > 0$ holds in the motoring mode, but in the regenerating mode at higher slips, it does not hold. Hence, the observer using the conventional adaptation law becomes unstable.

Based on Fig. 2, it can be noticed that the regenerating mode can be stabilized by changing the direction of the error projection. Consequently, the proposed adaptation law (7) in the estimated rotor flux reference frame is considered. The current estimation error is rotated by factor $\exp(-j\phi)$. Since the conventional adaptation law works well in the motoring mode, the angle ϕ is selected as

$$\phi = \begin{cases} \phi_{\max}\,\mathrm{sign}(\omega_s)\left(1 - \frac{|\omega_s|}{\omega_\phi}\right), & \text{if } \omega_s\hat{\omega}_r < 0 \text{ and } |\omega_s| < \omega_\phi \\ 0, & \text{otherwise} \end{cases} \tag{11}$$

where $\hat{\omega}_r = \omega_s - \hat{\omega}_m$ is the slip frequency estimate. For the given motor, $\phi_{\max} = 0.44\pi$ (i.e., 80°) and $\omega_\phi = 0.4$ p.u. were chosen. In Fig. 2, the current error locus resulting from (11) consists of the dash-dotted curve and the solid curve (the dash-dotted curve corresponding to the dashed curve rotated 78° around the origin). Now, the condition $i_{sq} - \hat{i}_{sq} > 0$ is valid for all slip frequencies.

Under the steady-state assumptions of this section, the parameters $\phi_{\max}$ and ω_ϕ can be substantially varied without losing the stability. The minimum value of ϕ, which stabilizes the speed estimation, is the value corresponding to $(\underline{i}_s - \hat{\underline{i}}_s)\exp(-j\phi)$ and $\hat{\underline{\psi}}_R$ being parallel. It was found out that the minimum stabilizing value of ϕ obtained using (9) is equal to the minimum value obtained using the linearized model in Section V. The maximum value of ϕ, on the other hand, is limited by the linearized model.

The proposed adaptation law is not restricted to the observer gain (4). Even the same values of $\phi_{\max}$ and ω_ϕ as for the observer gain (4) can be used in some cases, e.g., when using the observer gain proposed in [8] or the zero observer gain.

V. Linearized Model

The nonlinear and complicated dynamics of the speed-adaptive observer can be studied via small-signal linearization. The key factor in the linearization is to use a synchronous reference frame in order to obtain a steady-state operating point. In the linearized model, the dynamics of both the motor and the observer are taken into account. Even though the stator

dynamics are included in the model, the linearized model is independent of the stator voltage and, consequently, of the current controller. Accurate motor parameter estimates are assumed in the analysis. The controllers or the mechanical model are not included in the linearized model. This can be justified if the overall system can be divided into different time scales.

A. Estimation Error

In the rotor flux reference frame, the linearized small-signal model of (8a) becomes [10]

$$\dot{\underline{\mathbf{e}}} = (\underline{\mathbf{A}}_0 - \underline{\mathbf{L}}_0\mathbf{C})\,\underline{\mathbf{e}} + \begin{bmatrix} 0 \\ j\psi_{R0} \end{bmatrix}(\omega_m - \hat{\omega}_m) \tag{12a}$$

where $\underline{\mathbf{e}}$, ω_m, and $\hat{\omega}_m$ refer to the deviation about the operating point. The operating-point quantities are marked by the subscript 0, and the matrices are

$$\underline{\mathbf{A}}_0 = \begin{bmatrix} -\frac{1}{\tau'_s} - j\omega_{s0} & \frac{1}{\tau'_s} \\ \frac{1-\sigma}{\tau'_r} & -\frac{1}{\tau'_r} - j\omega_{r0} \end{bmatrix}, \quad \underline{\mathbf{L}}_0 = \begin{bmatrix} \underline{l}_{s0} \\ \underline{l}_{r0} \end{bmatrix} \tag{12b}$$

The transfer function from the estimation error of the speed $\omega_m - \hat{\omega}_m$ to the estimation error of the current $\underline{i}_s - \hat{\underline{i}}_s$ is

$$\begin{aligned} \underline{G}(s) &= \mathbf{C}\,(s\mathbf{I} - \underline{\mathbf{A}}_0 + \underline{\mathbf{L}}_0\mathbf{C})^{-1}\begin{bmatrix} 0 \\ j\psi_{R0} \end{bmatrix} \\ &= -\frac{j\psi_{R0}}{L'_s}\frac{s + j\omega_{s0}}{A(s) + jB(s)} \end{aligned} \tag{13a}$$

where $\mathbf{I} = \left[\begin{smallmatrix} 1 & 0 \\ 0 & 1 \end{smallmatrix}\right]$ is the identity matrix. The polynomials in (13a) are defined as

$$\begin{aligned} A(s) = {} & s^2 + s\left(\frac{1}{\tau'_s} + \frac{1}{\tau'_r} + \frac{l_{sd0} - l_{rd0}}{L'_s}\right) \\ & - \omega_{s0}\omega_{r0} + \frac{\sigma}{\tau'_s\tau'_r} + \frac{\omega_{s0}l_{rq0} - \omega_{r0}l_{sq0}}{L'_s} + \frac{\sigma l_{sd0}}{\tau'_r L'_s} \end{aligned} \tag{13b}$$

$$\begin{aligned} B(s) = {} & s\left(\omega_{s0} + \omega_{r0} + \frac{l_{sq0} - l_{rq0}}{L'_s}\right) \\ & + \frac{\omega_{s0}\tau'_s + \omega_{r0}\tau'_r}{\tau'_s\tau'_r} + \frac{\omega_{r0}l_{sd0} - \omega_{s0}l_{rd0}}{L'_s} + \frac{\sigma l_{sq0}}{\tau'_r L'_s} \end{aligned} \tag{13c}$$

where the entries of the observer gain are divided into real and imaginary components: $\underline{l}_{s0} = l_{sd0} + jl_{sq0}$ and $\underline{l}_{r0} = l_{rd0} + jl_{rq0}$. Since the observer gain is allowed to be a function of the estimated rotor speed, the subscript 0 is used. It is to be noted that $\underline{G}(s)$ is independent of the speed-adaptation law.

B. Closed-Loop System

1) Conventional Adaptation Law: Based on the conventional adaptation law (10), the linearized transfer function from the current error $i_{sq} - \hat{i}_{sq}$ to the speed estimate $\hat{\omega}_m$ is

$$K(s) = -\left(\gamma_p + \frac{\gamma_i}{s}\right)\psi_{R0} \tag{14}$$

Only the imaginary component $i_{sq} - \hat{i}_{sq}$ of the estimation error of the current is of interest. Thus only the imaginary component of (13a) is used,

$$G_q(s) = \mathrm{Im}\{\underline{G}(s)\} = -\frac{\psi_{R0}}{L'_s}\frac{sA(s) + \omega_{s0}B(s)}{A^2(s) + B^2(s)} \tag{15}$$

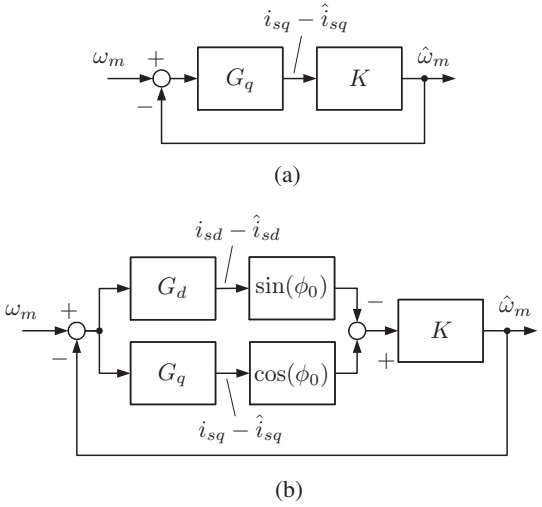

Fig. 3. Linearized model of observer: (a) conventional speed-adaptation law; (b) proposed speed-adaptation law.

Using (14) and (15), the closed-loop system shown in Fig. 3(a) is formed. The closed-loop transfer function corresponding to any operating point can be easily calculated using suitable computer software (e.g., MATLAB Control System Toolbox).

The pole plot of the linearized closed-loop system corresponding to the regenerating-mode operation is shown in Fig. 4(a). The slip frequency is $\omega_{r0} = -\omega_{rN}$. Only the dominant poles are shown. As assumed, the system is unstable at low stator frequencies (a real pole is located in the right half-plane). As shown in [3], the reason for the unstable closed-loop pole is the unstable zero of $G_q(s)$ in the regenerating mode at low speeds. As the feedback gain increases, the closed-loop poles move to the positions of the open-loop zeros [11, p. 175].

Even if high adaptation gains are used (and the assumption of slowly varying $\hat{\omega}_m$ made in Section IV is therefore not justified), the stability of the linearized model agrees with the results obtained in Section IV. The explanation is that the unstable zero of $G_q(s)$ is generally located close to the imaginary axis. Therefore, the unstable mode is slow compared with the dynamics of $\hat{\omega}_m$ during transients.

In order to illustrate the different time scales, simulation results of the linearized model of Fig. 3(a) are shown in Fig. 5. The (unstable) operating point is determined by $\omega_{s0} = 0.01$ p.u., $\omega_{r0} = -\omega_{rN}$, and $\psi_{R0} = 0.9$ Wb. A stepwise perturbation of $0.1\omega_{rN}$ is applied to the actual speed ω_m at $t = 0.1$ s. It can be seen that the transient response of the speed estimate $\hat{\omega}_m$ after $t = 0.1$ s is fast whereas the divergence of $\hat{\omega}_m$, caused by the unstable zero of $G_q(s)$, is very slow.

2) Proposed Adaptation Law: In the estimated rotor flux reference frame, the proposed error term (7) becomes

$$\varepsilon = \Big[(i_{sq} - \hat{i}_{sq})\cos(\phi) - (i_{sd} - \hat{i}_{sd})\sin(\phi)\Big]\,\hat{\psi}_R \tag{16}$$

The linearized system is shown in Fig. 3(b), where the transfer function from the estimation error of the speed $\omega_m - \hat{\omega}_m$ to the estimation error of the current $i_{sd} - \hat{i}_{sd}$ is

$$G_d(s) = \mathrm{Re}\{\underline{G}(s)\} = -\frac{\psi_{R0}}{L'_s}\frac{sB(s) - \omega_{s0}A(s)}{A^2(s) + B^2(s)} \tag{17}$$

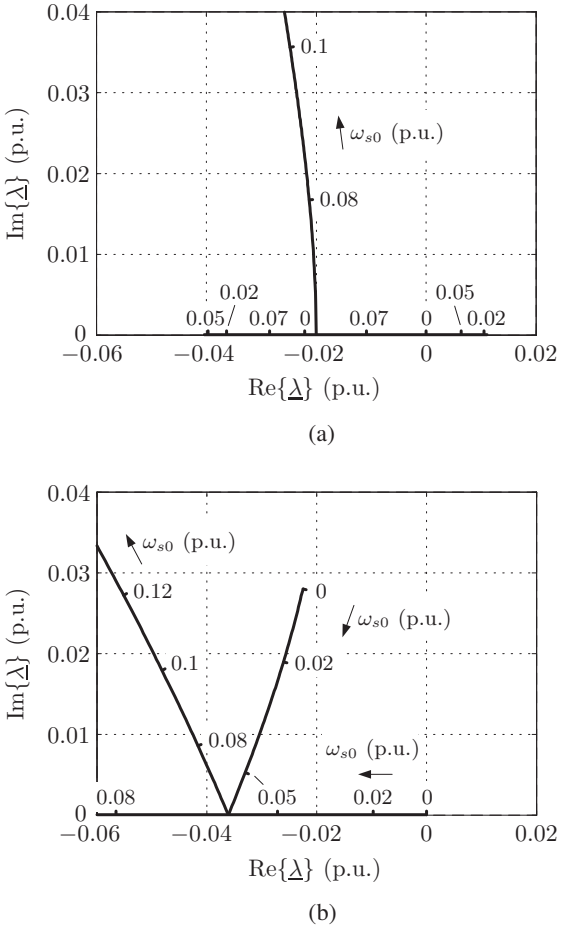

Fig. 4. Variation of dominant poles with stator frequency ω_{s0} in regenerating mode: (a) conventional adaptation law; (b) proposed adaptation law. Slip frequency is $\omega_{r0} = -\omega_{rN}$. Due to symmetry, only upper half-plane is shown.

Fig. 4(b) shows the pole plot of the linearized closed-loop system corresponding to the regenerating-mode operation. In this case, the system is also stable at low stator frequencies (marginally stable when the stator frequency is zero).

VI. Effect of Parameter Errors on Accuracy

The effect of parameter errors on the accuracy of the flux observer is crucial since it determines the robustness of the overall system [12]. The effect of erroneous parameters used within speed-adaptive flux observers can be studied by means of a steady-state expression for $\hat{\underline{\psi}}_R/\underline{\psi}_R$ [13]. In the following, the accuracy of the proposed observer design is compared with the accuracy of three existing observer designs [3], [5], [7], which reduce or remove the unstable region in the regenerating mode at low speeds if the parameter estimates are accurate. The state variables used in the compared observers differ from (3), and the transformation given in Appendix B is therefore used.

A steady-state solution of the rotor speed estimate $\hat{\omega}_m$ is required to determine $\hat{\underline{\psi}}_R/\underline{\psi}_R$. Since the error term ε of the speed-adaptation law is zero in steady state, the steady-state speed estimate can be found using iteration. Typically, more than one steady-state solution of $\hat{\omega}_m$ can be found, leading to more than one solution for $\hat{\underline{\psi}}_R/\underline{\psi}_R$. With realistic

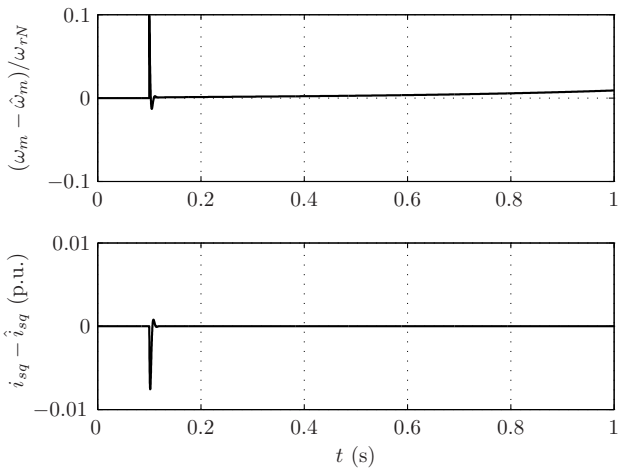

Fig. 5. Simulation of linearized small-signal model of Fig. 3(a). Unstable operating point is determined by $\omega_{s0} = 0.01$ p.u., $\omega_{r0} = -\omega_{rN}$, and $\psi_{R0} = 0.9$ Wb. Stepwise perturbation of $0.1\omega_{rN}$ is applied to actual speed ω_m at $t = 0.1$ s.

parameter errors, only one of the solutions fulfills the condition $\hat{\underline{\psi}}_R/\underline{\psi}_R \approx 1$ around the rated speed, whereas other solutions are far from unity. Considering observers capable to operate around the rated speed, it is clear that the rated-speed solution $\hat{\underline{\psi}}_R/\underline{\psi}_R \approx 1$ corresponds to the stable solution.

The approach used here is to find the solution $\hat{\underline{\psi}}_R/\underline{\psi}_R \approx 1$ at the rated speed. Then the speed is decreased, and the solution being continuous with the rated-speed solution is tracked. This process is continued until a discontinuity in the solution appears, or $\hat{\underline{\psi}}_R/\underline{\psi}_R = 0$ occurs. The same process is repeated starting from the negative rated speed. The described process generates the steady-state solutions of $\hat{\underline{\psi}}_R/\underline{\psi}_R$ that correspond to a very slow speed reversal starting from a higher speed (e.g., the rated speed) where $\hat{\underline{\psi}}_R/\underline{\psi}_R \approx 1$ holds.

The existence of a steady-state solution of $\hat{\underline{\psi}}_R/\underline{\psi}_R$ does not guarantee that the solution is stable. On the other hand, absence, discontinuity, or significant inaccuracy of a steady-state solution are clear indicators of stability problems. According to simulations and experiments, fast transients through the unstable regions are usually possible. The time that can be spent in the vicinity of the unstable region depends mainly on the accuracy of the stator resistance estimate.

The results obtained for different observer designs are described in the following subsections. The curves in Fig. 6(a,b,c,d) show the steady-state solutions of $\hat{\underline{\psi}}_R/\underline{\psi}_R$ when an erroneous stator resistance estimate is used. The curves in Fig. 6(e,f) depict the solutions of $\hat{\underline{\psi}}_R/\underline{\psi}_R$ corresponding to an erroneous magnetizing inductance estimate and an erroneous stator transient inductance estimate, respectively. In Fig. 6(a,b), the actual slip frequency $\omega_r = 0$ is used corresponding to no-load operation. In Fig. 6(c,d,e,f), the slip frequency used is equal to the rated slip, $\omega_r = \omega_{rN}$, corresponding approximately to the rated-load operation. The rotor resistance estimate has practically no effect on $\hat{\underline{\psi}}_R/\underline{\psi}_R$. The adaptation gains do not affect the steady-state expressions for $\hat{\underline{\psi}}_R/\underline{\psi}_R$.

When the slip frequency ω_r is zero, the solutions of $\hat{\underline{\psi}}_R/\underline{\psi}_R$ corresponding to the negative and positive stator frequencies

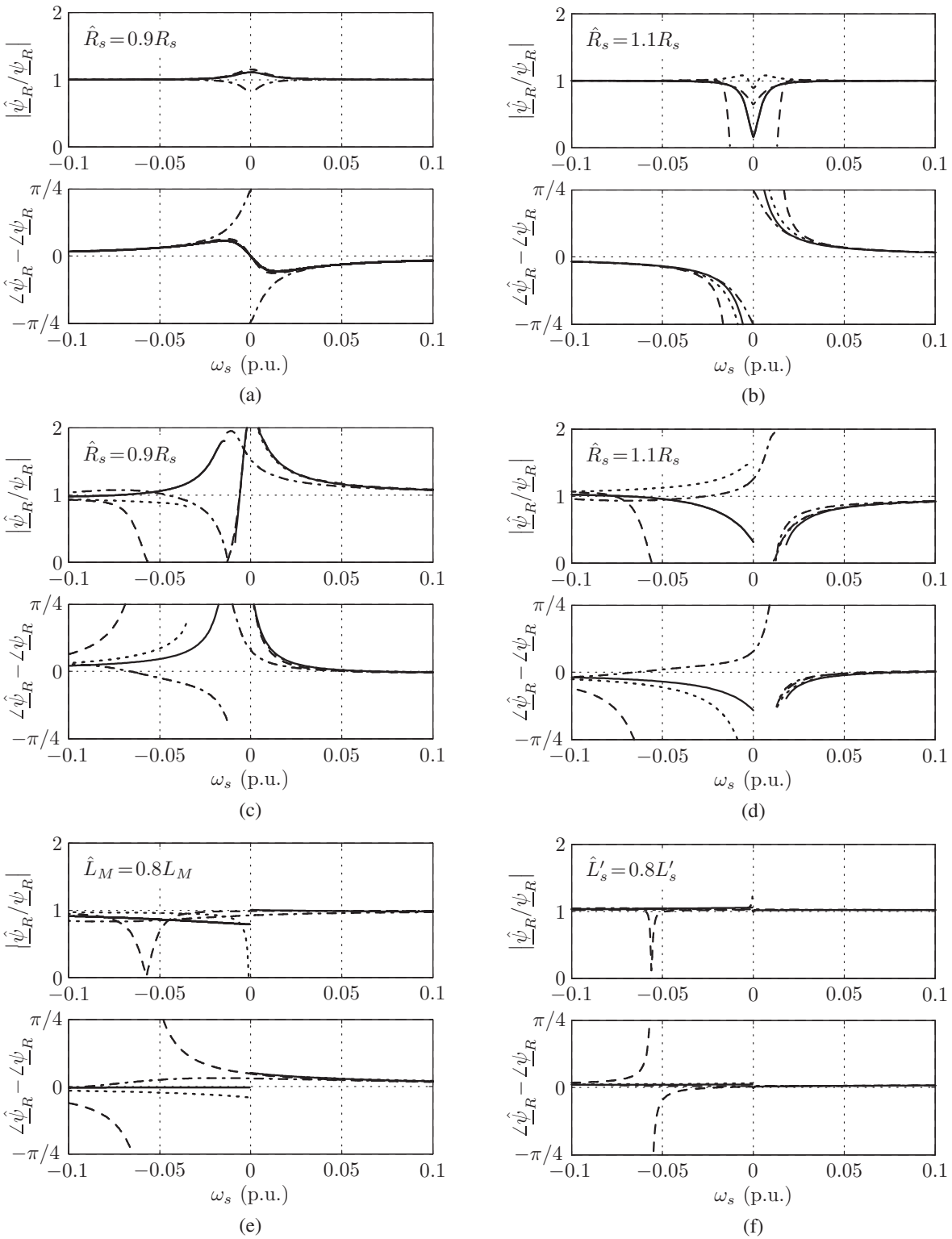

Fig. 6. Effect of parameter errors on $\hat{\underline{\psi}}_R/\underline{\psi}_R$: (a,b) actual slip frequency is $\omega_r = 0$; (c,d,e,f) $\omega_r = \omega_{rN} = 0.05$ p.u. Solid line corresponds to proposed observer, dashed line to observer described in Subsection VI-A, dotted line to observer described in Subsection VI-B, and dash-dotted line to observer described in Subsection VI-C. Observer parameters are marked by symbol $\hat{}$.

are symmetrical. For nonzero slip frequency, the solutions of $\underline{\hat{\psi}}_R/\underline{\psi}_R$ in the regenerating mode ($\omega_s\omega_r < 0$) and in the motoring mode are generally different. The operating point corresponding to zero rotor speed is found at the frequency $\omega_s = 0$ in Fig. 6(a,b) and at $\omega_s = \omega_{rN} = 0.05$ p.u. in Fig. 6(c,d,e,f).

A. Constant Observer Gain — Conventional Adaptation Law

The stability conditions for the speed-adaptive observer are analyzed in [3] when the conventional speed-adaptation law (6) is used. In order to reduce (not totally remove) the unstable region, a real-valued observer gain

$$\underline{\mathbf{L}} = [0 \quad l_r]^T \tag{18}$$

was considered. The parameter $l_r = -0.25R_s$ is selected here, corresponding to the simulations and experiments in [3]. The dashed curves in Fig. 6 show the steady-state solutions of $\underline{\hat{\psi}}_R/\underline{\psi}_R$. The unstable region in the regenerating mode can be clearly seen in Fig. 6(c,d,e,f). It is to be noted that the curves corresponding to zero observer gain are similar, except that the unstable region is larger and shifted to slightly higher absolute stator frequencies.

Based on the curves in Fig. 6(c,d,e,f), steady-state rated-load operation should be possible at zero speed even with slightly inaccurate parameter estimates. Based on Fig. 6(a,b), no-load operation at zero speed is possible if the stator resistance is underestimated (or accurate) but the overestimated stator resistance causes problems. Actually, there is a solution fulfilling the condition $\underline{\hat{\psi}}_R/\underline{\psi}_R \approx 1$ at very low speeds, but that solution is discontinuous with the desirable rated-speed solution and, therefore, not shown in Fig. 6(b). Steady-state operation at zero frequency is practically impossible under the rated load torque, as opposed to no-load operation.

B. Variable Observer Gain — Conventional Adaptation Law

If the dynamics of the speed-adaptation loop are ignored, a pole placement approach can be used to design the observer gain. Under this assumption, the observer poles (in the stator reference frame) are placed in proportion to the motor poles[1] using the observer gain [1]

$$\underline{\mathbf{L}} = (k-1)\, R_s \begin{bmatrix} k+1 \\ k - \frac{\tau'_s}{\tau'_r} + j\tau'_s\hat{\omega}_m \end{bmatrix} \tag{19a}$$

where a proportional factor $k = 1$ was originally selected (leading to $\underline{\mathbf{L}} = [0 \quad 0]^T$). As realized later [5], the dynamics of the speed adaptation has to be taken into account when designing the observer gain. The unstable region in the regenerating mode is removed by selecting the proportional factor as

$$k = \begin{cases} \frac{1}{2}\frac{\omega_s}{\hat{\omega}_m}\left(1 + \frac{\tau'_s}{\tau'_r}\right), & \text{if } \omega_s\hat{\omega}_r < 0 \\ 1, & \text{otherwise} \end{cases} \tag{19b}$$

The conventional speed-adaptation law (6) is used. The dotted curves in Fig. 6 depict the steady-state solutions of $\underline{\hat{\psi}}_R/\underline{\psi}_R$. It can be seen that the observer using (19) is more accurate than the observer described in Subsection VI-A.

[1]Disregarding the dynamics of the speed-adaptation loop, constant observer poles could easily be obtained. The observer gain, however, becomes inexpediently large at low speeds.

C. Zero Observer Gain — Modified Adaptation Law

In [7], the error term of the speed-adaptation law

$$\varepsilon = \mathrm{Im}\left\{\left(\underline{i}_s - \underline{i}_{sc}\right)\left(\underline{\hat{i}}_s - \underline{i}_{sc}\right)^*\right\} \tag{20a}$$

was proposed, where

$$\underline{i}_{sc} = \frac{R_s - j\omega_s\left(\frac{L_M}{2} + L'_s\right)}{R_s^2 + (L_M + L'_s)L'_s\omega_s^2}\underline{u}_s \tag{20b}$$

The current $\underline{i}_{sc}$ depending on the operating point corresponds to the center point of the current locus when the slip frequency is varied. Therefore, the sign of the angle between vectors $\underline{i}_s - \underline{i}_{sc}$ and $\underline{\hat{i}}_s - \underline{i}_{sc}$ corresponds to the sign of the speed estimation error. The observer gain $\underline{\mathbf{L}} = [0 \quad 0]^T$ is used. The dash-dotted curves in Fig. 6 show the steady-state solutions of $\underline{\hat{\psi}}_R/\underline{\psi}_R$. The accuracy in no-load operation is poor as can be seen in Fig. 6(a,b). The accuracy under rated load is comparatively good, especially in the plugging mode (where $\omega_m\omega_s < 0$) in Fig. 6(c) and in the regenerating mode (where $\omega_r\omega_s < 0$) in Fig. 6(d).

D. Proposed Design

The solid curves in Fig. 6 depict the steady-state expressions for $\underline{\hat{\psi}}_R/\underline{\psi}_R$ corresponding to the proposed observer design. The accuracy in no-load operation and in the motoring mode corresponds approximately to the accuracy of the observers described in Subsections VI-A and VI-B, whereas the proposed design is more accurate in the regenerating mode. Compared with the observer described in Subsection VI-C, the accuracy in the rated-load operation is slightly worse but the accuracy in no-load operation is much better.

Based on Fig. 6(c,d), the overestimated stator resistance results in better accuracy in the regenerating mode than the underestimated stator resistance does. Based on Fig. 6(a,b,c,d), the underestimated stator resistance gives better results in no-load operation and in the plugging mode operation. In the motoring mode, the steady-state performance is not strongly dependent on the sign of the stator resistance error.

The steady-state accuracy was not considered in the design phase of the proposed observer. It is assumed that the accuracy could be made even better by modifying the observer gain and the angle ϕ.

VII. Control System

The regenerating-mode low-speed operation of the speed-adaptive observer was investigated by means of simulations and experiments. The MATLAB/Simulink environment was used for the simulations. The experimental setup is shown in Fig. 7. The 2.2-kW four-pole induction motor (IM) was fed by a frequency converter controlled by a dSpace DS1103 PPC/DSP board.

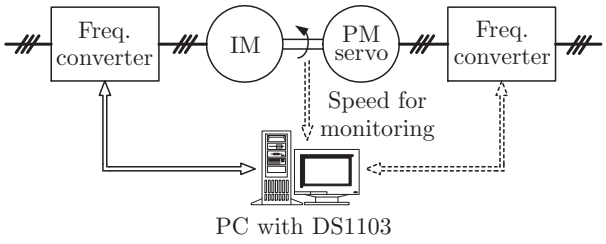

Fig. 7. Experimental setup. Permanent magnet (PM) servo motor was used as loading machine.

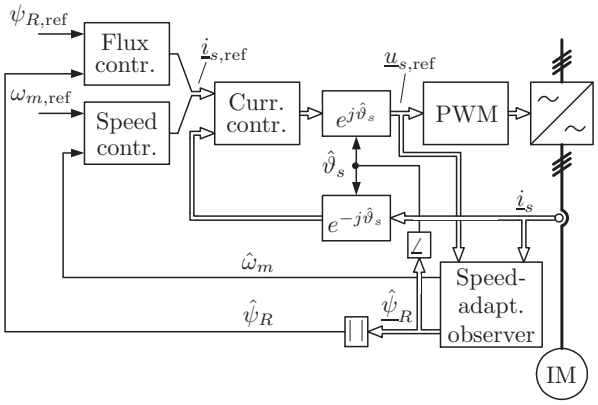

Fig. 8. Rotor flux oriented controller. Electrical variables shown on left-hand side of coordinate transformations are in estimated flux reference frame and variables on right-hand side are in stator reference frame.

The control system was based on the rotor flux orientation. The simplified overall block diagram of the system is shown in Fig. 8. The flux reference was 0.9 Wb. A PI-type synchronous-frame current controller was used [14]. The bandwidth of the current controller was 8 p.u. (where the base value is $2\pi{\cdot}50$ s^{-1}). The speed estimate was filtered using a first-order low-pass filter having the bandwidth of 0.8 p.u., and the speed controller was a conventional PI-controller having the bandwidth of 0.16 p.u. The flux controller was a PI-type controller having the bandwidth of 0.016 p.u.

The sampling was synchronized to the modulation and both the switching frequency and the sampling frequency were 5 kHz. The dc-link voltage was measured, and the reference voltage obtained from the current controller was used for the flux observer. A simple current feedforward compensation for dead times and power device voltage drops was applied [15].

VIII. Results

The base values used in the following figures are: current $\sqrt{2}{\cdot}5.0$ A and flux 1.0 Wb. Experimental results obtained using the conventional adaptation law and the observer gain (4) are shown in Fig. 9(a). The speed reference was set to 0.08 p.u. and a negative rated-load torque step was applied at $t = 1$ s. After applying the negative load, the drive should operate in the regenerating mode. However, the actual flux of the motor collapses soon after the torque step and the system becomes unstable. According to the pole plot in Fig. 4(a), the operating point is unstable since the stator frequency is approximately 0.05 p.u. Fig. 9(b) depicts experimental results obtained using

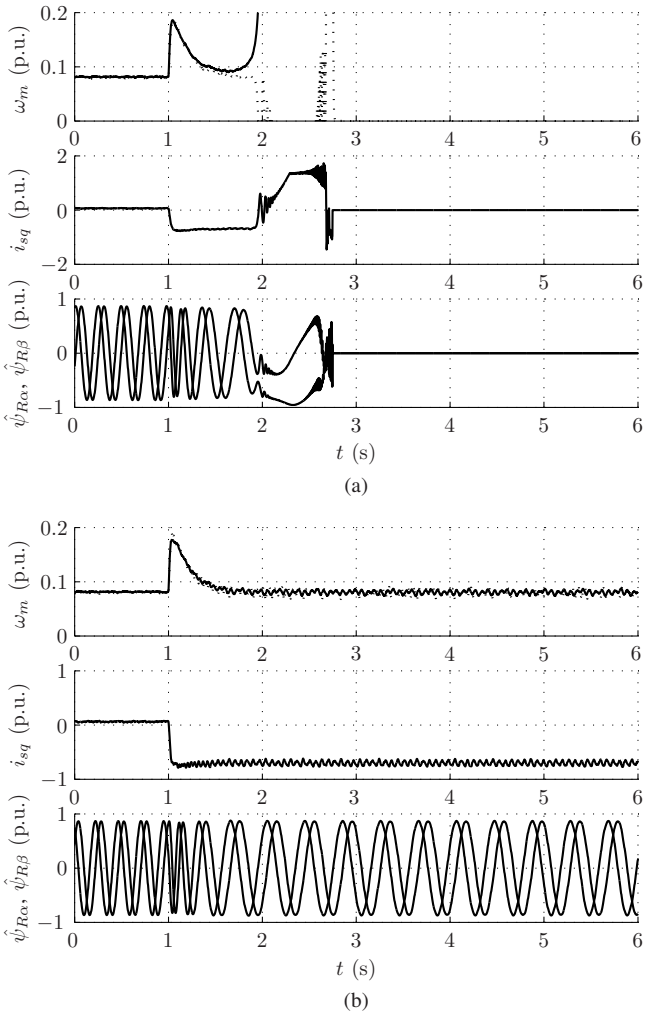

Fig. 9. Experimental results in regenerating mode when negative rated-load torque step is applied: (a) instability phenomenon with conventional speed-adaptation law and observer gain (4); (b) its remedy by using proposed observer design. Speed reference was set to 0.08 p.u. First subplot shows measured speed (solid) and estimated speed (dotted). Second subplot shows q component of stator current in estimated flux reference frame. Third subplot presents real and imaginary components of estimated rotor flux in stator reference frame.

the proposed observer design. As expected based on the pole plot in Fig. 4(b), the system behaves stably.

Further experimental results obtained using the proposed observer design are shown in Fig. 10. The speed reference was now set to 0.04 p.u. and a negative rated-load torque step was applied at $t = 5$ s. Even though the stator frequency is only about 0.0085 p.u., both the flux and speed are correctly observed.

Simulation results showing slow speed reversals are shown in Fig. 11(a). The proposed observer design was used. A rated-load torque step was applied at $t = 1$ s. The speed reference was slowly ramped from 0.06 p.u. ($t = 5$ s) to -0.06 p.u. ($t = 20$ s) and then back to 0.06 p.u. ($t = 35$ s). The drive operates first in the motoring mode, then in the plugging mode ($t \approx 12.5 \ldots 17.5$ s), in the regenerating mode ($t \approx 17.5 \ldots 22.5$ s), again in the plugging mode ($t \approx 22.5 \ldots 27.5$ s), and finally again in the motoring mode. Corresponding experimental results are shown in Fig. 11(b). The noise in

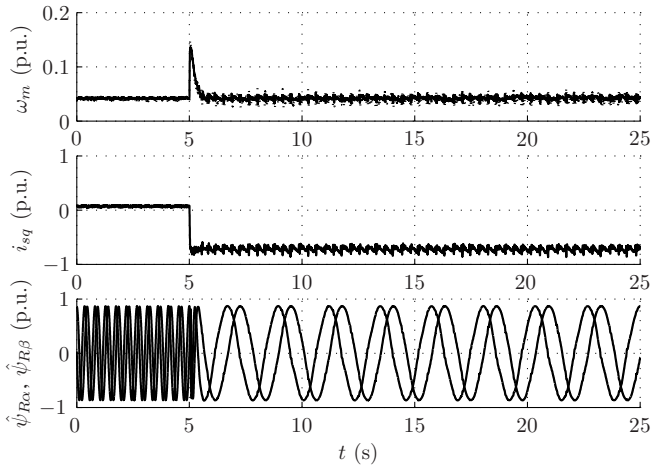

Fig. 10. Experimental results in the regenerating mode when negative rated-load torque step is applied. Proposed observer design was used. Speed reference was set to 0.04 p.u. Explanations of curves are as in Fig. 9.

the current and the speed estimate originates mainly from incomplete dead-time compensation. At a given speed, the proportional effect of the dead-time compensation is more significant in the regenerating mode than in the motoring mode since the amplitude of the stator voltage is smaller. As can be realized based on Fig. 6(c,d), this kind of speed reversals require a very accurate stator resistance estimate (error of only few percent allowed) since the stator frequency remains in the vicinity of zero for a long time.

Experimental results showing zero-speed operation and a rated-load torque step are shown in Fig. 12. The speed reference was set to zero. A rated-load torque step was applied at $t = 4$ s, and the load torque was removed at $t = 12$ s. It can be seen that both the flux and the speed are correctly observed. After removing the load, the flux is still properly estimated and the load torque could be applied again.

If the system becomes unstable due to overly inaccurate motor parameter estimates, the magnitude of the actual flux either collapses (leading to the disappearance of the electromagnetic torque), or the magnitude of the actual flux increases and the stator frequency locks on to a constant value [16]. To a certain extent, the steady-state expressions for $|\hat{\underline{\psi}}_R/\underline{\psi}_R|$ shown in Fig. 6 can be used to predict which instability phenomenon is more probable[2]. A suitable topic for future research is to investigate whether a stator resistance adaptation scheme can be incorporated without impairing stability. Alternatively, the sign of the stator resistance error could be taken into account in the observer design [16], [17]. This may require the stator resistance to be intentionally underestimated or overestimated.

IX. Conclusions

The conventional speed-adaptive flux observer has an unstable region in the regenerating mode at low speeds. In the observer design proposed in this paper, the speed-adaptation law is modified in the regenerating mode by exploiting the component of the current estimation error parallel to the estimated rotor flux in addition to the perpendicular component.

[2]If a flux controller is used, $|\hat{\underline{\psi}}_R/\underline{\psi}_R| = \psi_{R,\mathrm{ref}}/\psi_R$ in steady state.

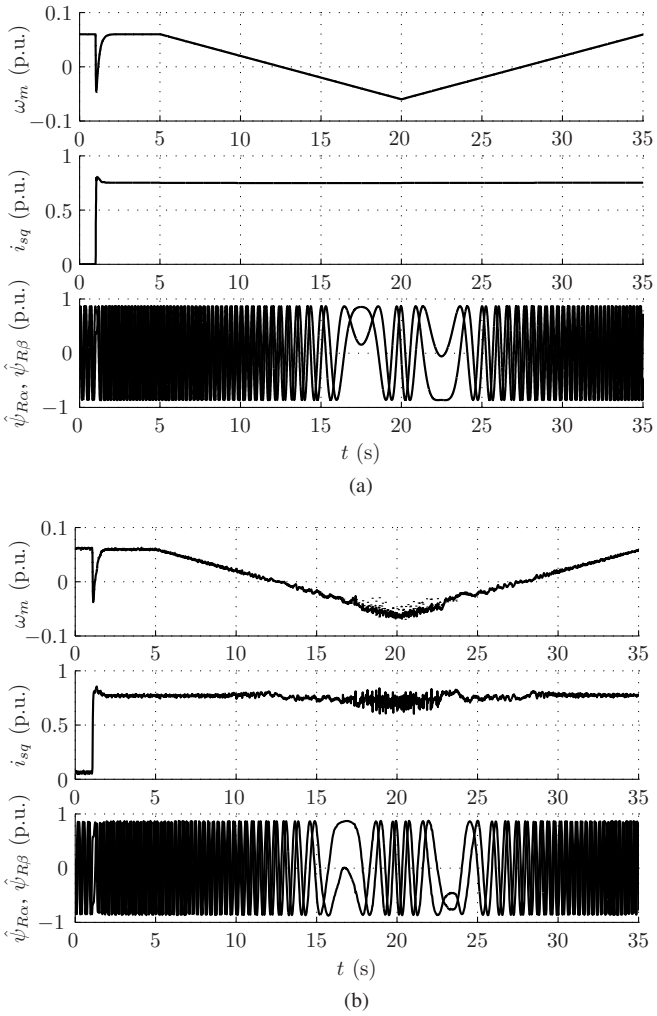

Fig. 11. Slow speed reversals when rated-load torque is applied: (a) simulation results; (b) experimental results. Proposed observer design was used. Explanations of curves are as in Fig. 9.

The observer using the proposed adaptation law does not have the unstable region, which was shown by means of current estimation error loci and a linearized model. The effect of parameter errors on the accuracy of the proposed observer is comparatively small. The stability of the regenerating-mode operation was also confirmed by simulations and experiments.

Appendix A
Global Stability of an Adaptation Law

The motor model (1) in the rotor reference frame (where $\omega_k = \omega_m$) was considered in [8], and a Lyapunov function candidate was chosen as

$$V = \frac{1}{2}\left[\gamma \underline{\mathbf{e}}^H \mathbf{P} \underline{\mathbf{e}} + (\omega_m - \hat{\omega}_m)^2\right] \tag{21}$$

where γ is a positive constant, the complex conjugate transpose is marked by the superscript H, and a symmetric real-valued positive definite matrix $\mathbf{P}$ was defined as

$$\mathbf{P} = \mathbf{\Gamma}^T\mathbf{\Gamma} = \begin{bmatrix} \frac{1}{L'_s} & -\frac{1}{L'_s} \\ 0 & 1 \end{bmatrix}^T \begin{bmatrix} \frac{1}{L'_s} & -\frac{1}{L'_s} \\ 0 & 1 \end{bmatrix} \tag{22}$$

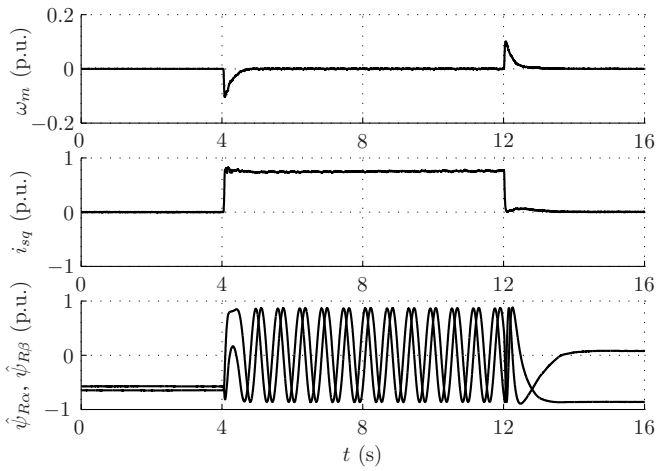

Fig. 12. Experimental results showing zero-speed operation when rated-load torque step is applied. Proposed observer design was used. Explanations of curves are as in Fig. 9.

Assuming $\dot{\omega}_m = 0$, the time derivative of V becomes

$$\dot{V} = \frac{\gamma}{2}\underline{\mathbf{e}}^H \underline{\mathbf{Q}}\underline{\mathbf{e}} + (\omega_m - \hat{\omega}_m)\left[\frac{\gamma}{L'_s}\,\mathrm{Im}\Big\{\big(\underline{i}_s - \hat{\underline{i}}_s\big)\underline{\hat{\psi}}_s^*\Big\} + \dot{\hat{\omega}}_m\right] \tag{23}$$

where the Hermitian matrix[3] $\underline{\mathbf{Q}}$ is

$$\begin{aligned}\underline{\mathbf{Q}} &= (\underline{\mathbf{A}} - \underline{\mathbf{L}}\mathbf{C})^H \mathbf{P} + \mathbf{P}\,(\underline{\mathbf{A}} - \underline{\mathbf{L}}\mathbf{C}) \\ &= \mathbf{\Gamma}^H\left[\big(\mathbf{\Gamma}\,(\underline{\mathbf{A}} - \underline{\mathbf{L}}\mathbf{C})\,\mathbf{\Gamma}^{-1}\big)^H + \mathbf{\Gamma}\,(\underline{\mathbf{A}} - \underline{\mathbf{L}}\mathbf{C})\,\mathbf{\Gamma}^{-1}\right]\mathbf{\Gamma}\end{aligned} \tag{24}$$

The speed adaptation law was obtained by zeroing the last term of (23). Therefore, the adaptation law is stable if the matrix $\underline{\mathbf{Q}}$ is negative semidefinite. However, unlike otherwise stated in [8], the semidefiniteness of $\underline{\mathbf{Q}}$ is not generally satisfied (albeit the eigenvalues of $\underline{\mathbf{A}} - \underline{\mathbf{L}}\mathbf{C}$ have negative real parts). Therefore, the stability of the adaptation law is not proved.

Appendix B
Transformation of Observer Gains

Conventionally, the stator current and the rotor flux are used as state variables in full-order flux observers [1], leading to

$$\dot{\hat{\underline{\mathbf{z}}}} = \hat{\underline{\mathbf{F}}}\,\hat{\underline{\mathbf{z}}} + \mathbf{G}\underline{u}_s + \underline{\mathbf{K}}\big(\underline{i}_s - \hat{\underline{i}}_s\big) \tag{25a}$$

$$\hat{\underline{i}}_s = \mathbf{H}\hat{\underline{\mathbf{z}}} \tag{25b}$$

where the observer state vector is $\hat{\underline{\mathbf{z}}} = [\hat{\underline{i}}_s \quad \underline{\hat{\psi}}_R]^T$, the observer gain is $\underline{\mathbf{K}} = [\underline{k}_s \quad \underline{k}_r]^T$, and $\mathbf{H} = [1 \quad 0]$. The matrices $\hat{\underline{\mathbf{F}}}$ and $\mathbf{G}$ are given by

$$\hat{\underline{\mathbf{F}}} = \begin{bmatrix} -\frac{1}{\tau'_\sigma} - j\omega_k & \frac{1}{L'_s}\left(\frac{1}{\tau_r} - j\hat{\omega}_m\right) \\ R_R & -\frac{1}{\tau_r} - j\,(\omega_k - \hat{\omega}_m) \end{bmatrix}, \quad \mathbf{G} = \begin{bmatrix} \frac{1}{L'_s} \\ 0 \end{bmatrix} \tag{25c}$$

where $\tau_r = L_M/R_R$ and $\tau'_\sigma = L'_s/(R_s + R_R)$. It can be easily shown that the transformation

$$\underline{\mathbf{K}} = \begin{bmatrix} \frac{1}{L'_s} & -\frac{1}{L'_s} \\ 0 & 1 \end{bmatrix}\underline{\mathbf{L}} \tag{26}$$

gives identical behavior to observers (3) and (25).

[3]Hermitian matrices are a generalization of symmetric matrices for complex matrices ($\underline{\mathbf{Q}} = \underline{\mathbf{Q}}^H$ holds), and they have real eigenvalues.

Acknowledgment

This work was financed in part by ABB Oy and in part by the Finnish Cultural Foundation. The authors would like to thank the reviewers for their professional work and helpful suggestions, and Prof. A. Medvedev for his valuable comments.

References

[1] H. Kubota, K. Matsuse, and T. Nakano, "DSP-based speed adaptive flux observer of induction motor," *IEEE Trans. Ind. Applicat.*, vol. 29, no. 2, pp. 344–348, Mar./Apr. 1993.

[2] G. Yang and T.-H. Chin, "Adaptive-speed identification scheme for a vector-controlled speed sensorless inverter-induction motor drive," *IEEE Trans. Ind. Applicat.*, vol. 29, no. 4, pp. 820–825, July/Aug. 1993.

[3] S. Suwankawin and S. Sangwongwanich, "A speed-sensorless IM drive with decoupling control and stability analysis of speed estimation," *IEEE Trans. Ind. Electron.*, vol. 49, no. 2, pp. 444–455, Apr. 2002.

[4] H. Tajima, G. Guidi, and H. Umida, "Consideration about problems and solutions of speed estimation method and parameter tuning for speed-sensorless vector control of induction motor drives," *IEEE Trans. Ind. Applicat.*, vol. 38, no. 5, pp. 1282–1289, Sept./Oct. 2002.

[5] H. Kubota, I. Sato, Y. Tamura, K. Matsuse, H. Ohta, and Y. Hori, "Regenerating-mode low-speed operation of sensorless induction motor drive with adaptive observer," *IEEE Trans. Ind. Applicat.*, vol. 38, no. 4, pp. 1081–1086, 2002.

[6] L. Harnefors, "Instability phenomena and remedies in sensorless indirect field oriented control," *IEEE Trans. Power Electron.*, vol. 15, no. 4, pp. 733–743, July 2000.

[7] H. Hofmann and S. R. Sanders, "Speed-sensorless vector torque control of induction machines using a two-time-scale approach," *IEEE Trans. Ind. Applicat.*, vol. 34, no. 1, pp. 169–177, Jan./Feb. 1998.

[8] J. Maes and J. A. Melkebeek, "Speed-sensorless direct torque control of induction motors using an adaptive flux observer," *IEEE Trans. Ind. Applicat.*, vol. 36, no. 3, pp. 778–785, May/June 2000.

[9] G. R. Slemon, "Modelling of induction machines for electric drives," *IEEE Trans. Ind. Applicat.*, vol. 25, no. 6, pp. 1126–1131, Nov./Dec. 1989.

[10] M. Hinkkanen, "Analysis and design of full-order flux observers for sensorless induction motors," *IEEE Trans. Ind. Electron.*, vol. 51, no. 5, pp. 1033–1040, Oct. 2004.

[11] S. Skogestad and I. Postlethwaite, *Multivariable Feedback Control: Analysis and Design*. Chichester, U.K.: John Wiley & Sons, 1996.

[12] P. L. Jansen and R. D. Lorenz, "A physically insightful approach to the design and accuracy assessment of flux observers for field oriented induction machine drives," *IEEE Trans. Ind. Applicat.*, vol. 30, no. 1, pp. 101–110, Jan./Feb. 1994.

[13] M. Hinkkanen and J. Luomi, "Parameter sensitivity of full-order flux observers for induction motors," *IEEE Trans. Ind. Applicat.*, vol. 39, no. 4, pp. 1127–1135, July/Aug. 2003.

[14] F. Briz, M. W. Degner, and R. D. Lorenz, "Analysis and design of current regulators using complex vectors," *IEEE Trans. Ind. Applicat.*, vol. 36, no. 3, pp. 817–825, May/June 2000.

[15] J. K. Pedersen, F. Blaabjerg, J. W. Jensen, and P. Thogersen, "An ideal PWM-VSI inverter with feedforward and feedback compensation," in *Proc. EPE'93*, vol. 4, Brighton, U.K., Sept. 1993, pp. 312–318.

[16] R. Ottersten, "On control of back-to-back converters and sensorless induction machine drives," Ph.D. dissertation, Dept. Elect. Pow. Eng., Chalmers Univ. Tech., Göteborg, Sweden, 2003.

[17] J. Kim, K. Nam, J. Chung, and H. Sunwoo, "Sensorless vector control scheme for induction motors based on a stator flux estimator with quadrant error compensation rule," *IEEE Trans. Ind. Applicat.*, vol. 39, no. 2, pp. 492–503, Mar./Apr. 2003.

Marko Hinkkanen was born in Rautjärvi, Finland, in 1975. He received the M.Sc. degree in electrical engineering in 2000 from Helsinki University of Technology, Espoo, Finland, where he is currently working toward the D.Sc. degree.

Since 2000, he has been with the Power Electronics Laboratory, Helsinki University of Technology, as a research scientist. His main research interest is the control of electrical drives.

Jorma Luomi (M'92) was born in Helsinki, Finland, in 1954. He received his M.Sc. (Eng.) and D.Sc. (Tech.) degrees from Helsinki University of Technology in 1977 and 1984, respectively.

In 1980 he joined Helsinki University of Technology, and from 1991 to 1998 he was a Professor at Chalmers University of Technology. As of 1998 he holds the position of Professor at the Department of Electrical and Communications Engineering at Helsinki University of Technology. His research interests are in the areas of electric drives, electric machines and numerical analysis of electromagnetic fields.